Facile enhancement of bulk heterojunction solar cells performance by utilizing PbSe nanorods decorated with graphene

E.M. El-Menyawy, L. Cattin, J.C. Bernède, Guy Louarn, Ludovic Arzel

Version of Record: https://www.sciencedirect.com/science/article/pii/S0021979719306836
Manuscript_d43620c179b28f93bbfe178cb9cb2682

Facile enhancement of bulk heterojunction solar cells performance by utilizing PbSe nanorods decorated with graphene

E.M. El-Menyawy[a,b*], L. Cattin[a], J.C. Bernède[c], Guy Louarn[a], Ludovic Arzel[a]

[a]Institut des Matériaux Jean Rouxel (IMN), CNRS, UMR 6502, Université de Nantes, 2 rue de la Houssinière, BP 32229, 44322 Nantes cedex 3, France.
[b]Solid State Electronics Laboratory, Solid State Physics Department, Physics Research Division, National Research Centre, 33 El-Bohouth St., Dokki, Giza 12622, Egypt.
[c]MOLTECH-Anjou, CNRS, UMR 6200, Université de Nantes, 2 rue de la Houssinière, BP 92208, Nantes, F-44000 France.

Abstract

An efficient approach for improving the photoelectrical conversion efficiency (PCE) of the bulk heterojunction (BHJ) solar cells, based on poly(3-hexylthiophene) (P3HT) and [6,6]-phenyl-C_{61} butyric acidmethyl ester ($PC_{61}BM$), by the incorporating PbSe nanorods decorated with graphene (G) into their active layer has been reported for the first time. Pristine PbSe and PbSe:G composites (with different amount of graphene) are synthesized via hydrothermal process and the formation mechanism is explained. The systematic investigation indicates that the crystallite size of PbSe:G increases with increasing graphene content. The PCE of the classical BHJ solar cells based on P3HT:$PC_{61}BM$ is improved from 2.32 up to 2.57 % by the incorporation of pristine PbSe. It is also enhanced by the incorporation of PbSe:G up to certain composition of graphene in which a maximum PCE value of 5.16 % is achieved. The external quantum efficiency of the BHJ solar cells is also investigated. The photovoltaic parameters are discussed based on the morphology variation detected by scanning electron microscope and atomic force microscope of the active layer together with their UV-VIS absorption measurements.

Keywords: BHJ solar cells; PbSe nanorods; Graphene; surface morphology; optical absorption.

*Corresponding author: Tel.: +2 01006021326

E-mail address: emad_elmenyawy@yahoo.com (E.M. El-Menyawy)

1. Introduction

The world is currently witnessing remarkable progress in the architecture of solar cells due to the emerging demand for energy, which is obviously reflected in the significant jump in their photoelectrical conversion efficiency (PCE). On classification, inorganic solar cells like Si and $CuInSe_2$ based materials have delivered high PCE, but they suffer from high cost contracting the demand for mass production. On contrast, organic based solar cell like solution-processable bulk heterojunction (BHJ) solar cells possess several positive features such as low cost and ease of fabrication on different substrates and even on cloths[1,2].

The traditional BHJ solar cells consisting of conducting polymers such as poly(3-hexylthiophene) (P3HT) as electron donor and fullerene derivatives such as [6,6]-phenyl-C_{61} butyric acid methyl ester ($PC_{61}BM$) as electron acceptor are considered as vital model for BHJ solar cells. The idea behind this combination is to utilize two different components, with different electron affinities and ionization potentials, to facilities exciton dissociation [3]. The huge scientific research concerning this type of solar cells arises from the fact that the best performance has not been reached yet. A theoretical model based on optimizing conditions specially the electronic levels, band gap and charge carriers mobility indicated that the PCE can approaches 11 % [4]. Despite the positive features of this type of solar cells, the major problem is being the low mobility of the organic materials which hinders the charge carriers transport and motives their recombination and

subsequently limits their performance [5-7]. In this regard, several strategies have been employed to overcome this problem. One of the key issues to improve the charge carrier mobility of the active layer is to utilize the inorganic nanocrystals such as PbSe [8], CdSe [9] and FeS_2[10] which result also in the enhancement of charge carrier separation by providing large interfacial area and better charge carries transport. Introducing highly conductive materials such as metals (Au [11] and Ag [12]) and graphene [13] into the active layer can be used as an important approach for providing the performance of the solar cells. Annealing at suitable temperatures is also found to be an important tool to increase the charge carriers mobility through improving the ordering of the active layer components [14]. Other studies have been dedicated to increase the PEC by using graphene oxide (GO) functionalized with conducting polymers [15] and Niobium doped ZnO nanorods [16].

The evolution of the different types of solar cells by the incorporation of graphene into their construction has recently been reviewed [17]. In this work, it is aimed to adapt a different strategy for realizing improved performance of BHJ solar cells. We utilize classical BHJ solar cells based on P3HT:PC_{61}BM as active layer and explore how to improve their performance by the addition of PbSe nanorods decorated with graphene in their active layer. The idea behind to use PbSe nanorods decorated with graphene in this matrix is to combine the advantage of PbSe for providing efficient charge carrier generation and transport. Nanorods can provide easier pathways for charge carriers more than spherical particles. In addition, graphene with its high mobility (~10^4 $cm^2V^{-1}s^{-1}$[18]) can also push towards this aim. Actually, it is realized that the decoration of FeS_2 nanocrystals

(NCs) with graphene can increase the photocurrent [19]. Besides, CdS decorated graphene was found to decrease the series resistance of the solar cells and subsequently to increase the PCE of the cells by more than 100 % compared to pristine cells [20].

2. Experimental

2.1 Synthesis of GO and PbSe:G nanocomposites

GO was prepared as described in our publication elsewhere [20]. The prepared GO was washed with distilled water until the pH reached 5. Then, the GO was dispersed in water and was sonicated for 2 hrs and finally dried at 70℃. PbSe nanorods was also prepared according to the procedure reported by us elsewhere [21] with slight modification. Typically, 0.07 g of polyethylene glycol (PEG) was dissolved in 70 mL of deionized water by magnetically stirring the solution. After complete dissolving, 2 mmole of both lead acetate trihydrate and sodium selenite were added to the solution with continuous stirring. A few minutes after, 20 mL of hydrazine hydrate was added to the mixture and the volume of total solution was completed to 100 mL by excess of deionized water. The solution was then transferred to a Teflon-linked stainless steel autoclave. The solution was heated at 110℃ for 12 hr. Then, the autoclave was left to cool to room temperature naturally and solid product was washed with distilled water, chloroform, methanol and pyridine several times, and then was dried at 70℃ for 6 hrs.

To prepare PbSe:G nanocomposites, different amounts was added to the mixture in-situ of preparing PbSe nanorods. The samples prepared with

the amounts of 0.005, 0.01 and 0.02 wt are denoted as PbSe:G1, PbSe:G2 and PbSe:G3, respectively though the paper.

2.2 Solar cells fabrication

ITO (glass/ITO) slides with a sheet resistance of 25 Ω/cm^2 were used for devices fabrication. A part of ITO coated glass substrates was removed by using a solution made from dust Zn dissolved in concentrated hydrochloric acid. To avoid removing all ITO covering the glass substrates, a major part of ITO-coated glass slides was masked with adhesive sheet. After etching, the adhesive sheet is removed and the substrates were washed several times with distilled water to remove the residuals. Then, the substrates were gently scrubbed with soap and rinsed several times with distilled water. Subsequently, the substrates were dried by air before inserting them inside the vacuum chamber to deposit a thin buffer layer from MoO_3.

P3HT used in this study was obtained from CODEX International, whereas $PC_{61}BM$ was obtained from Sigma-Aldrich. A 0.1 g of P3HT was dissolved in 5 mL of dichlorobenzene (20 mg/ml) by magnetic stirrer, and then $PC_{61}BM$ was added to the solution. The weight ratio of P3HT:$PC_{61}BM$ was kept as 1:1. The final solution was stirred in the dark for 20 h under heating temperature of 50℃. Thin films P3HT:$PC_{61}BM$ blend was deposited onto ITO/MoO_3 by using spin coating technique with a rotating speed of 10^3 rpm for two minutes. The active layers coated-ITO/MoO_3 were annealed at 140℃for 30 min under nitrogen environment. This heat treatment has a vital role of improving the photovoltaic properties of the devices based on P3HT:$PC_{61}BM$ as active layer [22]. Then, LiF film with a thickness of 1 nm was deposited on the active layer followed by the deposition of Al film with

a thickness of about 100 nm through a shadow mask to form the back contact electrode. LiF and Al films were deposited by using thermal evaporation technique without breaking the vacuum. The thickness of MoO_3, LiF and Al layers was controlled in-situ by quartz-crystal thickness monitor. The rate deposition of these layers was kept constant as 0.1 Å/s. The thermal deposition was performed at vacuum chamber of 10^{-4}Pa. The photoactive area of all devices was kept constant as 0.07 cm^2 for all the samples. A schematic diagram showing the solar cell structure is shown in Fig. 1. In order to prepare organic:inorganic active layers, 2 mg of PbSe, PbSe:G1, PbSe:G2 and PbSe:G3 were added individually to the P3HT:PC_{61}BM blend and magnetically stirred for the same period.

3.4 Characterization

The crystalline structure of pristine PbSe and PbSe decorated with graphene is identified with Panalytical Empyrean X-ray diffractometer model 202964 utilizing CuK_α radiation 1.5406 Å. The tube current and the accelerating voltage were 30 mA and 40 *kV*, respectively.

The morphology of the active layer of solar cells was investigated with field emission gun scanning electron microscope (SEM) JEOL 7600F. The images were taken at operating voltage of 5 *kV* and with secondary electron and backscattering detectors ("Centre de microcaractéristion, Institut des Matériaux Jean Rouxel, Université de Nantes"). The topography of the active layers was also checked with atomic force microscope (AFM) instrument (dimension Edge-Bruker) in tapping mode. The images were treated by means of WSXM software [23].

Optical absorbance measurements were recorded on a Perkin Elmer (Lambda 1050) spectrophotometer. The measurements were achieved at room temperature. The measurements were performed from the back side of the samples to be compatible with the solar cells measurements.

The electrical and photoelectrical current-voltage characteristics of the solar cells were recorded on Keithley 2601 source-meter. The solar cells were illuminated with a calibrated solar simulator (Oriel 300 W) at light intensity of 100 mW/cm^2 adjusted with 0.5 cm^2 CIGS reference solar cell calibrated at NREL, USA. The measurements were carried out under sun global AM 1.5 at room temperature. The illumination for the solar cells was performed from the ITO side.

3. Results and discussion

3.1 Synthesis and characterization of pristine PbSe and PbSe decorated with graphene

Fig. 2 depicts the XRD spectra of pristine PbSe and PbSe decorated with different amounts of graphene. The presence of different elevated peaks with different intensities indicates well crystalline nature of the prepared samples. The observed peaks are corresponding to the growth along (111), (200), (220), (311), (222) and (400) directions of PbSe cubic structure. The data were indexed according to the Standard data (03-065-1074). It can be observed that the general trend is the increase of the intensity of the peaks by increasing graphene content implying better crytallinity. No detection of other peaks corresponding to another phase rather than PbSe is observed implying obtaining pure product of PbSe. The average crystallite size, D, is

estimated using Scherrer formula as 36, 44, 48 and 55 nm for PbSe, PbSe:G1, PbSe:G2 and PbSe:G3, respectively. The general behavior indicates that the particle size increases with increasing graphene content. Besides, the common peak of G is not also detected which can be ascribed to its small amount to be detected by XRD technique.

Fig. 3 illustrates the morphology of pristine PbSe and PbSe decorated with different amount of graphene as detected with TEM. The image of pristine PbSe shows that it is grown as randomly distributed nanorods. The diameter of the rods is variable in which it lies between 23 and 115 nm. By the introduction of graphene, transparent sheets of graphene can be observed. In addition, cubic-shaped particles of PbSe are accumulated around the rods and this trend is clearly visible in the sample of higher graphene content. This accumulation is in accordance with the increase of crystallite size of the samples by increasing graphene content. The mechanism of PbSe formation can be described as follows:

On one hand, the lead acetate dissolves in excess deionized water according to the chemical equations:

$$Pb^{+2} + 2OH^{1} \rightarrow Pb(OH_2) \quad (1)$$

$$Pb(OH)_2 + 2(OH)^{-1} = Pb(OH)_4^{-2} \quad (2)$$

On the other hand, sodium selenite reacts with hydrazine hydrate according to the chemical equations:

$$3SeO_3^{-2} + 3(N_2H_4) \rightarrow 3Se + 3N_2 \uparrow + 3H_2O + 6(OH^-) \quad (3)$$

$$3Se + 6(OH^-) \rightarrow 2Se^{-2} + SeO_3^{-2} + 3H_2O \quad (4)$$

Then, the binary selenium ions from Eq. 4 react with the lead source from Eq. 2 resulting in the formation of PbSe according to:

$$Pb(OH)_4^{-2} + Se^{-2} \rightarrow PbSe\downarrow + 4(OH)^{-1} \quad (5)$$

Additionally, the formation mechanism of PbSe:G can be then explained. By the dispersing GO in water, it becomes negatively charged as a result of the ionization of both hydroxyl and carboxyl groups on its surface [24]. Accordingly, the negatively charged GO activate the adsorption of positively charged Pb^{+2} ions by the effect of electrostatic attraction. Finally, the GO can be reduced to graphene through the hydrothermal process by using hydrazine hydrate as reducing agent. From the forgoing discussion, as the concentration of GO increases, the surface active is increased resulting in enhanced nucleation which in turn leads to more accumulation and increased crystallite size.

3.2 Morphology of active layer films

The surface texture of P3HT/PC_{61}BM blend, spin-coated onto ITO/MoO_3, before and the addition of pristine PbSe and PbSe decorated with graphene are shown in Fig. 4. The top surface scan image of P3HT/PC_{61}BM shows very smooth surface revealing the formation of homogenously distributed P3HT/PC_{61}BM blend without voids or cracks. By embedding the pristine PbSe and PbSe:G1 into P3HT:PC_{61}BM blend, the surface of the blend is still homogenous without also voids and cracks. By adding PbSe:G2 to the organic blend, it can be observed that some heaps of

cubic and rod-shape PbSe are appeared at the surface. From this phenomenon, we can conclude that when the crystallinity of PbSe decorated with graphene attain certain value the particles segregate from the P3HT:PC_{61}BM blend towards the surface. This conclusion is supported by further increase of the graphene content (sample PbSe:G3) as this sample has higher degree of crystallinity.

For obtaining further insight into the morphology modification by the addition of PbSe and PbSe:G to the P3HT/PC_{61}BM blend, the AFM measurements are recorded and illustrated in Fig. 5. The morphology of the classical P3HT:PC_{61}BM deposited on ITO/MoO_3 shows spherical-like grains. These grains are distributed over all the measured area with a root-mean square (RMS) value of 7 nm. This value is relatively high, but it can be accepted specially that the films are fabricated with the spin coating technique. The insertion of pristine PbSe NCs in P3HT:PC_{61}BM blend results in a slight decrease in the value of RMS for the active layer to 8 nm. By the introduction with the graphene (sample P3HT:PC_{61}BM:PbSe:G1), the value of RMS is increased to 12 nm. From the image of P3HT:PC_{61}BM:PbSe:G2 composition, shiny grains from PbSe:G2 are appeared on the surface of the blend and the RMS value is estimated as 38 nm. By further increase of graphene content (P3HT:PC_{61}BM:PbSe:G3), the rod-like particles are observer and the value of RMS is further increased to 67 nm. The results show that the value of RMS increases with increasing the particle size of the samples.

3.3 Optical absorbance

The absorbance spectra of the P3HT, $PC_{61}BM$, P3HT:$PC_{61}BM$, pristine PbSe and P3HT:$PC_{61}BM$:PbSe films are represented in Fig. 6. It can be seen that the spectra of P3HT has a wide band of absorption concentrated specially in the visible light region over wavelength range 400-650 nm. The spectra of $PC_{61}BM$ show absorption in the wavelength range of 300-450 nm. It can be observed the spectra of P3HT:$PC_{61}BM$ can be considered as the sum of the absorption caused by the individual P3HT and $PC_{61}BM$ layers. The absorption of this layer is in accordance with the published data [25]. The absorption of PbSe is being in the wavelength range 300-630 nm together with an absorption background at wavelengths greater than 630 nm. Besides, the absorption due to P3HT:$PC_{61}BM$:PbSe blend represents the absorption sum of their individual layers.

Fig. 7 demonstrates the effect of introduction of graphene on the absorbance spectra of P3HT:$PC_{61}BM$:PbSe blend. It can be observed that the influence of the graphene addition on the absorbance curve of P3HT:$PC_{61}BM$:PbSe:G1 blend is marginal, whereas the spectra of the absorbance of P3HT:$PC_{61}BM$:PbSe:G2 is slightly decreased over the spectral range 300-650 nm, and there is an absorption background appeared at longer wavelengths. This is associated with the partial release of inorganic NCs to the surface of the active layer. The absorption spectra of P3HT:$PC_{61}BM$:PbSe:G3 is higher than that of P3HT:$PC_{61}BM$:PbSe:G2 and its absorption background is disappeared. With more release of PbSe NCs towards the surface, there is more chance for the organic components to absorb the light waves.

3.4 Photovoltaic properties

In all of the fabrication of the solar cell under investigation, a hole transporting layer form MoO_3 is used with a constant thickness between the ITO-coated glass and the active layer. Fig. 8a represents the cross-section image of ITO/MoO_3 film. It can be observed that the thickness of the MoO_3 layer is in the range of 8-10 nm. It is realized that a thin layer of MoO_3 with a thickness up to 10 nm can be used as a hole transporting layer in polymeric solar cells with an acceptable efficiency [26] specially that our target is not to obtain the optimum value of the PCE, but to investigate the possibility of the improvement of this value by introducing inorganic NCs decorated with graphene. The film thickness value of the active layer composed of P3HT:PC_{61}BM and P3HT:PC_{61}BM:PbSe:G2 as a representative samples is also estimated from the cross-section SEM images illustrated in Fig. 8b and Fig. 8c, respectively. The images show that the thickness of the former active layer is about 132 nm and is increased to about 155 for the later one.

The current density-volt (J-V) measurements under illumination of the devices based on pristine PbSe and PbSe decorated with graphene embedded in P3HT:PC_{61}BMblend are demonstrated in Fig. 9. The classical solar cell based on P3HT:PC_{61}BM as active layer is also included for comparison. The summary of the extracted photovoltaic parameters such as open-circuit voltage (V_{oc}), short-circuit current density (J_{sc}), Fill factor (FF), photoelectrical conversion efficiency (PCE), series resistance (R_s) and shunt resistance (R_{sh}) obtained for such cells are listed in Table 1. The values of R_s and R_{sh} were extracted as the inverse slope of the power curve tangent at open circuit voltage and the short-circuit current, respectively [27]. Besides, the value of FF and PCE were determined using classical expressions [28].

The classical solar cell based on P3HT:$PC_{61}BM$ shows PCE of 2.32 % with V_{oc} and J_{sc} values of 0.55 V and 9.03 mA/cm^2, respectively. The measurements reveal that by embedding the pristine PbSe into the P3HT:$PC_{61}BM$, the PEC value is increased to 2.57 %. This increase is mainly due to the increase in J_{sc} to 9.97 mA/cm^2. The value of FF is decreased due to the increase in the value of R_s. However, the increase of the R_s by the insertion of PbSe is unexpected owing to assumed high mobility of PbSe (0.7 $cm^2V^{-1}s^{-1}$[29]) compared to organic components. This increase compared to the cell based on only P3HT:$PC_{61}BM$ as active layer can be explained in terms of the presence of some traces of PEG linked to PbSe which acts as resistive component. This seems to contradict with the enhanced value of J_{sc} of the cell. For further analysis to assess the role of PbSe NCs in the improvement of the value of J_{sc} although there is an increase in the value of R_s, the external quantum efficiency (EQE) of the cells are measured and are illustrated in Fig. 10. The results indicate that the main contribution of the photocurrent to the device based on P3HT:$PC_{61}BM$ is in the range of 300-660 nm and the contribution of the PbSe NCs to the device based on P3HT:$PC_{61}BM$:PbSe is negligible which is in accordance with the absorption measurements. It is well-know that the theoretical EQE value arises from the product of photon absorption, carriers diffusion, carriers separation and finally carriers collection[30]. Thus, the increment in the value of J_{sc} for the cell based on P3HT:$PC_{61}BM$ by the introduction of PbSe NCs can be due to the efficient exciton dissociation and carrier transport.

The inclusion of the graphene with the first composition (Sample P3HT:$PC_{61}BM$:PbSe:G1) leads to a substantial increment in the device

performance in which the device delivers PCE of 4.55 %. This increment is mainly due to the increment in the value of J_{sc} up to 18.89 mA/cm^2 thanked to the high mobility of graphene. The increase of the particle size is also another reason for the evolution in the value of J_{sc}. These conclusions are drawn based on the observed decrease in the value of R_s. The device also shows a decrease in the value of R_{sh} which can be ascribed to the increase of the leakage current. Referring to the EQE curve of this cell, the curve is in accordance to the absorbance curve of the corresponding active layer. Hence, the increase of EQE can be ascribed mainly to the increase of the value of J_{sc}.

The solar cell based on the active layer of P3HT:PC_{61}BM:PbSe:G2 shows also enhanced performance with the optimum condition for PCE in showing PCE value of 5.16 %. In this case, the value of J_{sc} is slightly decreased be to 17.35 mA/cm^2 which can correlated to the decrease of the in the absorbance. Further decrease of the value of R_s is still present. This means that the contribution of the graphene with its high value of mobility together with the increase of PbSe:G2 crystallinity are still valid. The slight decrement of the value of J_{sc} can also be due to the partially release of the PbSe:G2 on the surface of the active layer which deceases the interfacial surface area responsible for charge carrier dissociation. This conclusion is assisted by the EQE in which the intensity of the curve is decreased for this cell compared to the previous composition.

The solar cell based on PbSe:G with high graphene content (P3HT:PC_{61}BM:PbSe:G3) shows a deterioration in the value of PCE as it obtained as 4.49 %. This deterioration is accompanied with the decrease of the value of J_{sc} which can be attributed to the increase of the corresponding

R_s value. The release of more PbSe NCs decorated with graphene on the surface of the active layer results in a negative contribution of the mobility of graphene to the effective active layer of the device which in turn results in an increase of the value of R_s. Lager particle size has also been observed to decrease the efficiency of BHJ solar cells based on P3HT:PbSe NCs as active layer due to the agglomeration of PbSe particles [31]. The decrease of the value of the J_{sc} is also supported by the decrease of the photocurrent observed from the EQE measurements. The device in this case has the optimum condition of the value of FF which reflected by the highest value of R_{sh}. Correlating solar cells parameters with the value of RMS and optical absorbance of the active layers indicate that although that the value of RMS increases with increasing graphene content and there is no significant increase in the absorbance curve, the value of PCE increases (except the last composition). This trend indicates that the effect of the high mobility of graphene is more effective for such cells.

4. Conclusion

PbSe nanorods decorated with graphene (PbSe:G) are successfully prepared by means of hydrothermal method. The crystallite size of PbSe is found to be 36 and increases as 44, 48 and 55 nm with the increase of GO concentration through the synthesis of PbSe:G composites. The inclusion of PbSe:G composites into the organic active layer (P3HT:$PC_{61}BM$) of the traditional BHJ solar cell shows positive effect in improving the value of PCE due to enhanced photocurrent thanks to the high charge carriers mobility of graphene which in turn enhance charge carriers transport and

suppress the recombination. The optical measurements show that there was no contribution of the PbSe:G composites to broaden the absorption range of the pure active layer. The crystallite size of PbSe:G composites and their blend with the active layer together with their morphology control the photocurrent. The overall development processes indicate the possibility of increment of PCE of BHJ solar cells through combining the positive futures of both graphene and inorganic NCs.

Acknowledgement

This work was supported by the French and Egyptian governments through a co-financed fellowship granted by the French embassy in Egypt (Institut Francais d'Egypte) and the Science and Technology Development Fund (STDF).

References

[1] S.-S. Kim, S.-I. Na, J. Jo, G. Tae, D.-Y. Kim, Efficient polymer solar cells fabricated by simple brush painting, Adv. Mater. 19 (2007) 4410–4415.

[2] Y.-J. Jeonb, J.-M. Yunc, D.-Y. Kimc, S.-I Nab, S.-S. Kima, Moderately reduced graphene oxide as hole transport layer in polymer solar cells via thermal assisted spray process, Applied Surface Science 296 (2014) 140–146.

[3] H. Spanggaard, F.C. Kerbs, A brief history of the development of organic and polymeric photovoltaics, Sol. Energy Mater. Sol. Cells 83 (2004) 125–146.

[4] L.J.A. Koster, V.D. Mihailetchi, P.W.M. Blom, Ultimate efficiency of polymer/fullerene bulk heterojunction solar cells, Appl. Phys. Lett. 88 (2006) 093511.

[5] G. Yu, J. Gao, J.C. Hummelen, F. Wudl, A.J. Heeger, Polymer photovoltaic cells: Enhanced efficiencies via a network of internal donor-acceptor heterojunctions, Science 270 (1995) 1789–1791.

[6] Y. Wang, W. Wei, X. Liu, Y. Gu, Sol. Energy Mater. Sol. Cells 98 (2012) 129–145.

[7] Z. Wang, S. Qu, X. Zhang, M. Shi, F. Tan, Z. Wang, J. Liu, Y. Hou, F. Teng, Z. Feng, Synthesis of MDMO-PPV capped PbS quantum dots and their applications to solar cells, Polymer 49 (2008) 4647–4651.

[8] Y. Sun, Z. Liu, J. Yuan, J. Chen, Y. Zhou, X. Huang, W. Ma, Polymer selection toward efficient polymer/PbSe planar heterojunction hybrid solar cells, Organic Electronics 24 (2015) 263–271.

[9] F.A. Roghabadi, M. Kokabi, V. Ahmadi, G. Abaeiani, Structure optimization of P3HT:CdSe hybrid solar cell using optical analysis and electrochemical impedance spectroscopy, Thin Solid Films 621 (2017) 19–25.

[10] C.W. Lin, D.Y. Wang, Y.T. Wang, C.C. Chen, Y.J.Yang, Y.F. Chen, Increased photocurrent in bulk-heterojunction solar cells mediated by FeS_2 nanocrystals, Sol. Energy Mater. Sol. Cells 95 (2011) 1107–1110.

[11] S.W. Heo, E.J. Lee, K.W. Song, J.Y. Lee, D.K. Moon, Enhanced carrier mobility and photon-harvesting property by introducing Au nano-particles in bulk heterojunction photovoltaic cells, Organic Electronics 14 (2013) 1931–1938.

[12] B.V.K. Naidu, J.S. Park, S.C. Kim, S.-M. Park, E.-J. Lee, K.-J. Yoon, S.J. Lee, J.W. Lee, Y.-S. Gal, S.-H. Jin, Novel hybrid polymer photovoltaics made by generating silver nanoparticles in polymer/fullerene bulk heterojunction structures, Sol. Energy Mater. Sol. Cells 92 (2008) 397–401.

[13] F. Zabihi, Q. Chen, Y. Xie, M. Eslamian, Fabrication of efficient graphene-doped polymer/fullerene bilayer organic solar cells in air using spin coating followed by ultrasonic vibration post treatment, Superlattices and Microstructures 100 (2016) 1177–1192.

[14] Y.-H. Lee, W.-C. Chen, C.-J. Chiang, K.-C. Kau, W.-S. Liou, Y.-P. Lee, L. Wang, C.-A. Dai, A new strategy for fabricating organic photovoltaic devices with stable D/A double-channel network to enhance performance using self-assembling all-conjugated diblock copolymer, Nano Energy13(2015) 103–116.

[15] C.K. Lyu, F. Zheng, B.H. Babu, M.S. Niu, L. Feng, J.L. Yang, W. Qin, X.T. Hao, Functionalized graphene oxide enables high-performance bulk heterojunction organic solar cell with a thick active layer, J. Phys. Chem. Lett. 9 (2018) 6238- 6248.

[16] H. Naz, R.N. Ali, Q. Liu, S. Yang, B. Xiang, Niobium doped zinc oxide nanorods as an electron transport layer for high-performance inverted polymer solar cells, J. Colloid Interface Sci. 512 (2018) 548–554.

[17] M.Z. Iqbal, A.-U. Rehman, Recent progress in graphene incorporated solar cell devices, Solar Energy 169 (2018) 634–647.

[18] A. Nikolakopoulou, D. Tasis, L. Sygellou, P. Lianos, Dispersion of graphene in organic solvents and their use for improving efficiency of dye- and quantum dot-sensitized solar cells, Electrochimica Acta 139 (2014) 54–60.

[19] C.W. Lin , D.Y. Wang, Y.T. Wang, C.C. Chen, Y.J. Yang , Y.F. Chen, Increased photocurrent in bulk-heterojunction solar cells mediated by FeS_2 nanocrystals, Sol. Energy Mater. Sol. Cells 95 (2011) 1107–1110.

[20] E.M. El-Menyawy, I.T. Zedan, A.A. Azab, One-pot solvothermal synthesis and characterization of CdS nanotubes decorated with graphene for solar cell applications, Journal of Alloys and Compounds 695 (2017) 3429–3434.

[21] E.M. El-Menyawy, G.M. Mahmoud, S.A. Gad, A.A. Azab, F.S. Terra, Dependence of the structural, electrical and optical properties of PbSe nanomaterial prepared by hydrothermal method on the polyethylene glycol content, J. Inorg. Organomet Polym 25 (2015) 1044–1052.

[22] Y. Jouane, S. Colis, G. Schmerber, P. Kern, A. Dinia, T. Heiser, Y.-A. Chapuis, Room temperature ZnO growth by rf magnetron sputtering on top of photoactive P3HT:PCBM for organic solar cells, J. Mater. Chem. 21 (2011) 1953–1958.

[23] I. Horcas, R. Fernandez, J.M. Gomez-Rodriguez, J. Colchero, J. Gomez-Herrero, A.M. Baro, WSXM: A software for scanning probe microscopy and a tool for nanotechnology, Rev. Sci.Instrum. 78 (2007) 013705.

[24] D. Li, M.B. Muller, S. Gilje, R.B. Kaner, G.G. Wallace, Processable aqueous dispersions of graphene nanosheets, Nat. Nanotechnol. 3 (2008) 101–105.

[25] S.W. Heo, I.S. Song, Y.S. Kim, D.K. Moon, FabricationofOPVsbyintroducingaconductivity-enhancedhybridbuffer layer, Sol. Energy Mater. Sol. Cells101(2012)295–302.

[26] V. Shrotriya, G. Li, Y. Yao, C.-W. Chu, Y. Yanga, Transition metal oxides as the buffer layer for polymer photovoltaic cells, Applied Physics Letters 88 (2006) 073508.

[27] Z. El Jouad, L. Barkat, N. Stephant, L. Cattin, N. Hamzaoui, A. Khelil, M. Ghamnia, M. Addou, M. Morsli, S. Béchu, C.Cabanetos, M. Richard-Plouet, P. Blanchard, J.C. Bernède, Ca/Alq_3 hybrid cathode buffer layer for the optimization of organic solar cells based on a planar heterojunction, Journal of Physics and Chemistry of Solids 98 (2016) 128–135.

[28] E. M. El-Menyawy, Electrical and photovoltaic properties of Gaussian distributed inhomogeneous barrier based on tris(8-hydroxyquinoline) indium/p-si interface, Materials Science in Semiconductor Processing, 32 (2015) 145–151.

[29] M. Nam, S. Kim, M. Kang, S.-W. Kim, K.-K. Lee, Efficiency enhancement in organic solar cells by configuring hybrid interfaces with narrow bandgap PbSSe nanocrystals, Organic Electronics 13 (2012) 1546–1552.

[30] P. Mao, Y. Wei, H. Li, J. Wang, Junction diodes in organic solar cells, Nano Energy 41 (2017) 717–730.

[31] K.P. Fritz, S. Guenes, J. Luther, S. Kumar, N.S. Sariciftci, G.D. Scholes, IV–VI Nanocrystal–polymer solar cells, Journal of Photochemistry and Photobiology A: Chemistry 195 (2008) 39–46.

Figures caption

Fig. 1 Schematic diagram of the BHJ solar cells.

Fig. 2 XRD patterns of: (a) pristine PbSe, (b) PbSe:G1, PbSe:G2 and PbSe:G3.

Fig. 3 TEM images of: (a) pristine PbSe, (b) PbSe:G1, PbSe:G2 and PbSe:G3.

Fig. 4 SEM surface images of active layers deposited on ITO/MoO_3: (a) P3HT:PC_{61}BM, (b) P3HT:PC_{61}BM:PbSe, (c) P3HT:PC_{61}BM:PbSe:G1, (d) P3HT:PC_{61}BM:PbSe:G2 and (e) P3HT:PC_{61}BM:PbSe:G3.

Fig. 5 Tapping-mode AFM surface topography of active layers deposited on ITO/MoO3: (A) P3HT:PC61BM, (B) P3HT:PC61BM:PbSe, (C) P3HT:PC61BM:PbSe:G1, (D) P3HT:PC61BM:PbSe:G2 and (E) P3HT:PC61BM:PbSe:G3. The corresponding three dimensional (3D) images for A, B, C, D and E are denoted as A3D, B3D, C3D, D3D and E3D, respectively.

Fig. 6 Absorbance spectra of: (a) P3HT, (b) PC_{61}BM, (c) P3HT:PC_{61}BM, (d) PbSe and (e) P3HT:PC_{61}BM:PbSe.

Fig. 7 Absorbance spectra of: (a) P3HT:PC_{61}BM:PbSe, (b) P3HT:PC_{61}BM:PbSe:G1, (c) P3HT:PC_{61}BM:PbSe:G2 and (d) P3HT:PC_{61}BM:PbSeG3.

Fig. 8 Cross-section SEM images shows the film thickness of: (a) MoO_3 layer, (b) P3HT:PC_{61}BM layer and (c) P3HT:PC_{61}BM:PbSe:G2 layer.

Fig. 9 J-V characteristics of BHJ solar cells depending on different active layers.

Fig. 10 EQE characteristics of BHJ solar cells depending on different active layers.

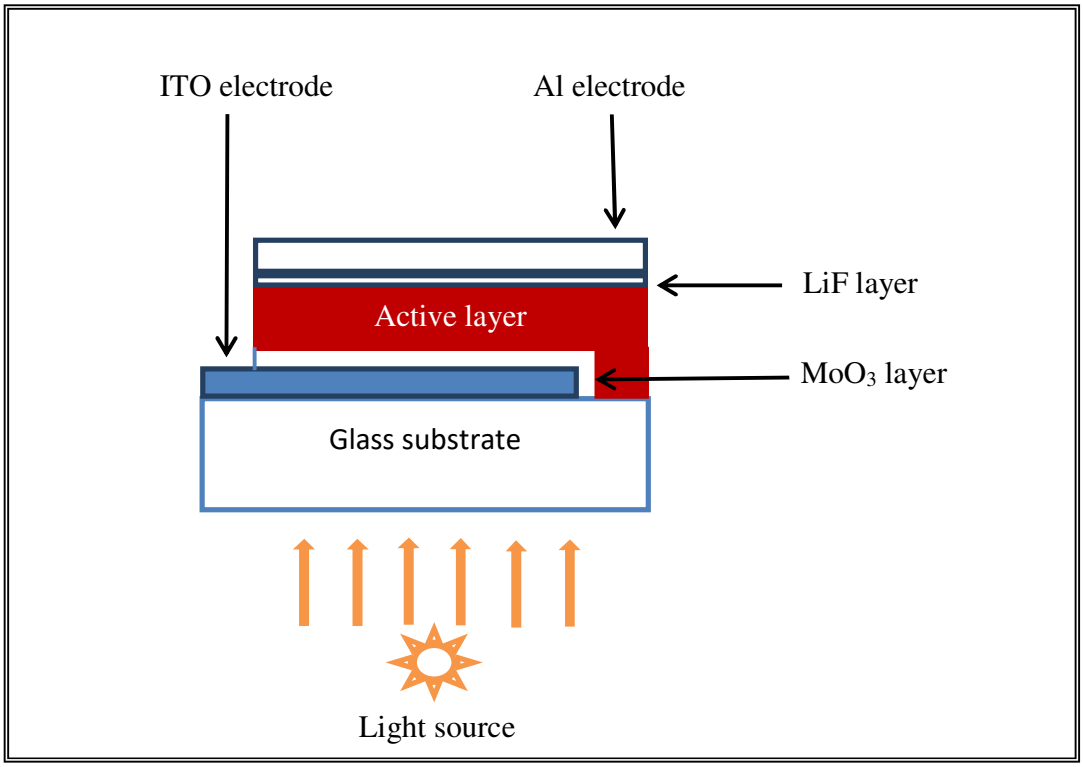
ITO electrode
Al electrode
LiF layer
Active layer
MoO_3 layer
Glass substrate
Light source

Fig. 1

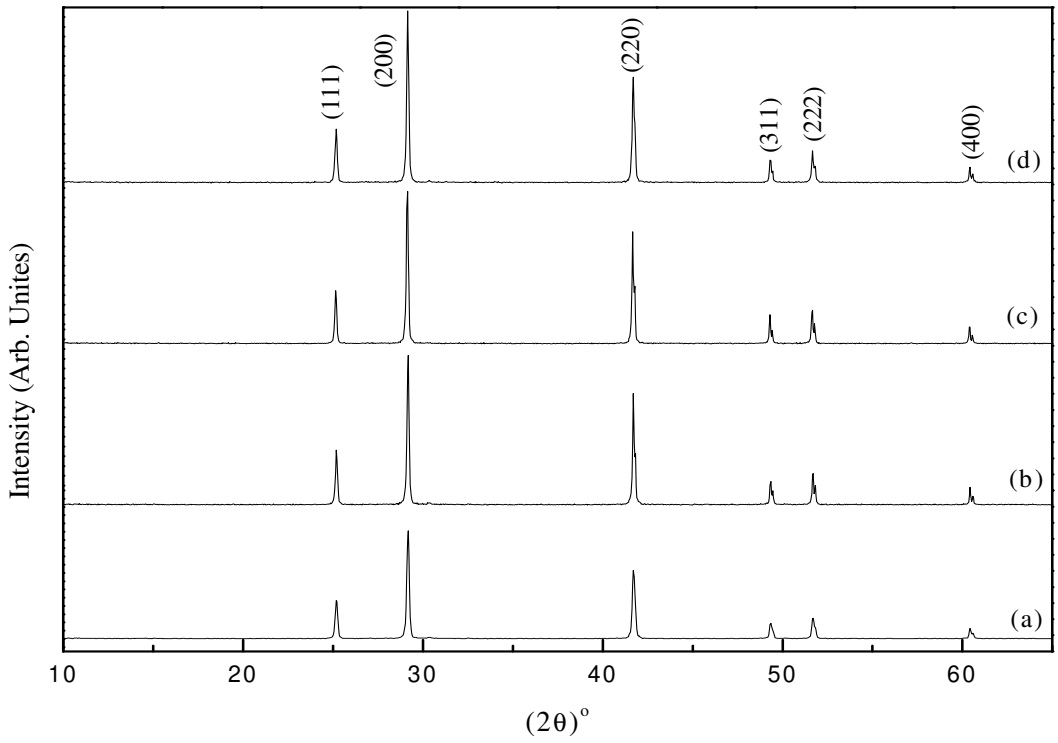
(111)
(200)
(220)
(311)
(222)
(400)
(d)
(c)
(b)
(a)
Intensity (Arb. Unites)
10
20
30
40
50
60
(2θ)°

Fig. 2

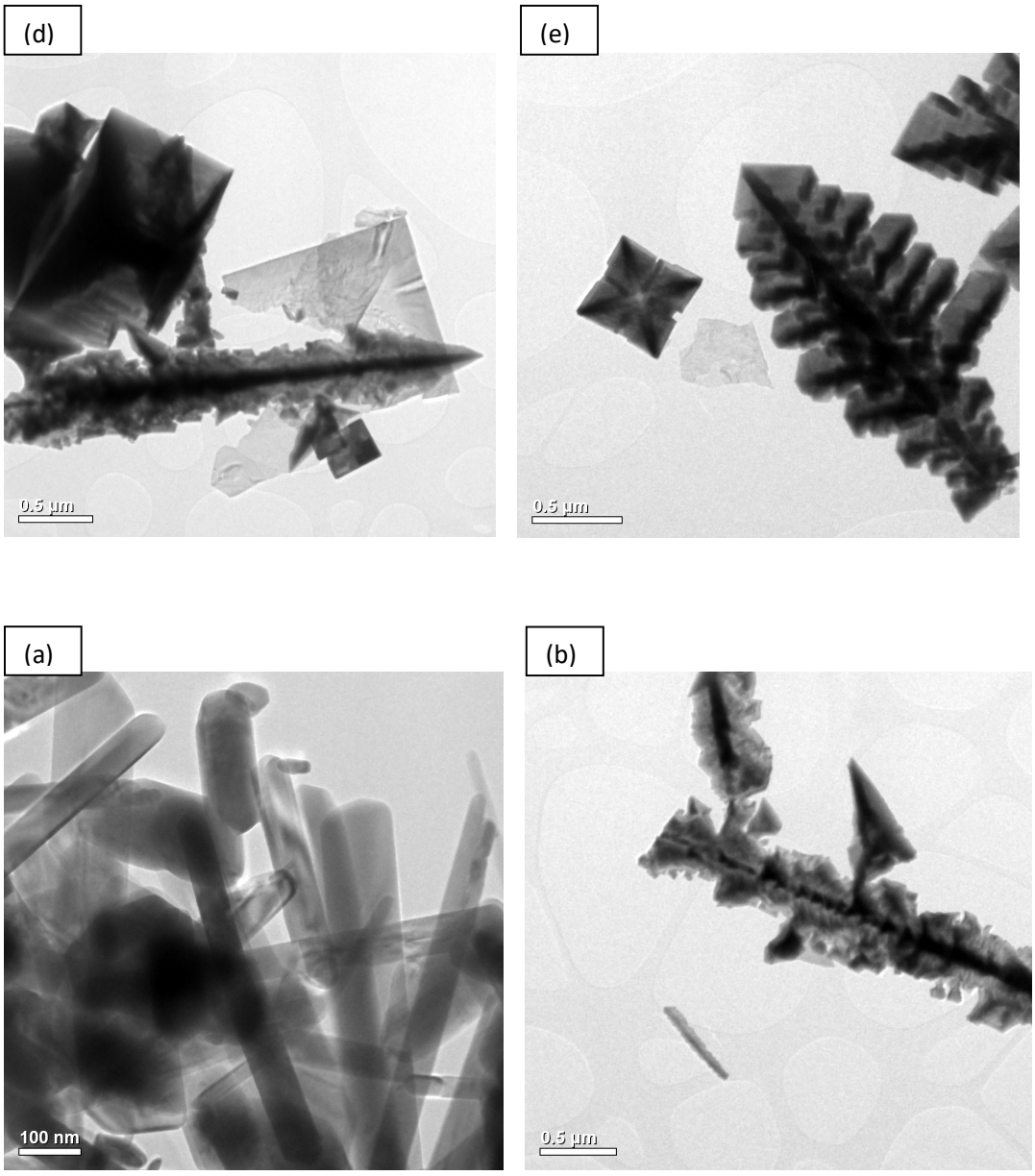

Fig. 3

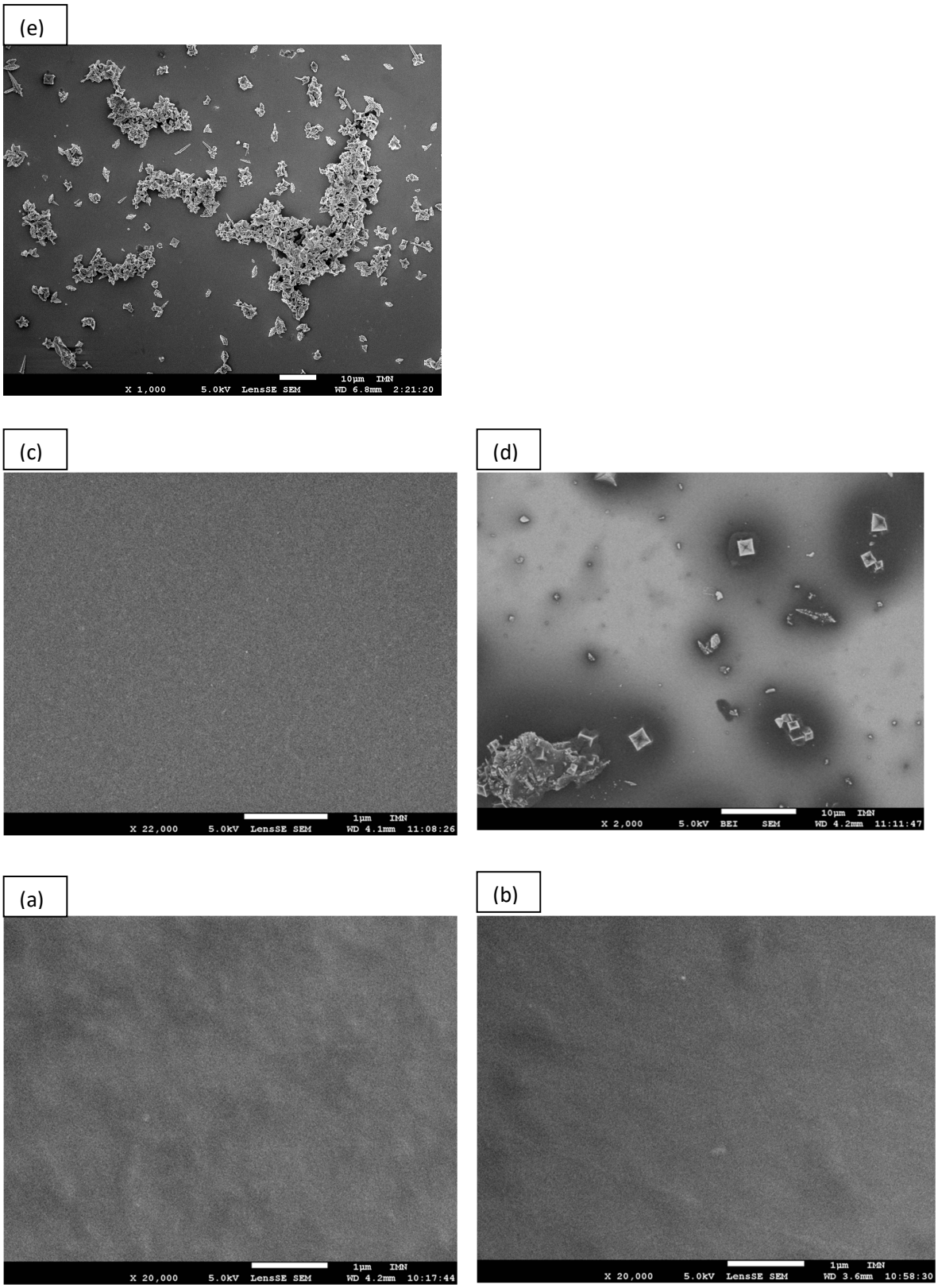
(e)
X 1,000 5.0kV LensSE SEM 10µm IMN WD 6.8mm 2:21:20
(c)
X 22,000 5.0kV LensSE SEM 1µm IMN WD 4.1mm 11:08:26
(d)
X 2,000 5.0kV BEI SEM 10µm IMN WD 4.2mm 11:11:47
(a)
X 20,000 5.0kV LensSE SEM 1µm IMN WD 4.2mm 10:17:44
(b)
X 20,000 5.0kV LensSE SEM 1µm IMN WD 3.6mm 10:58:30

Fig. 4

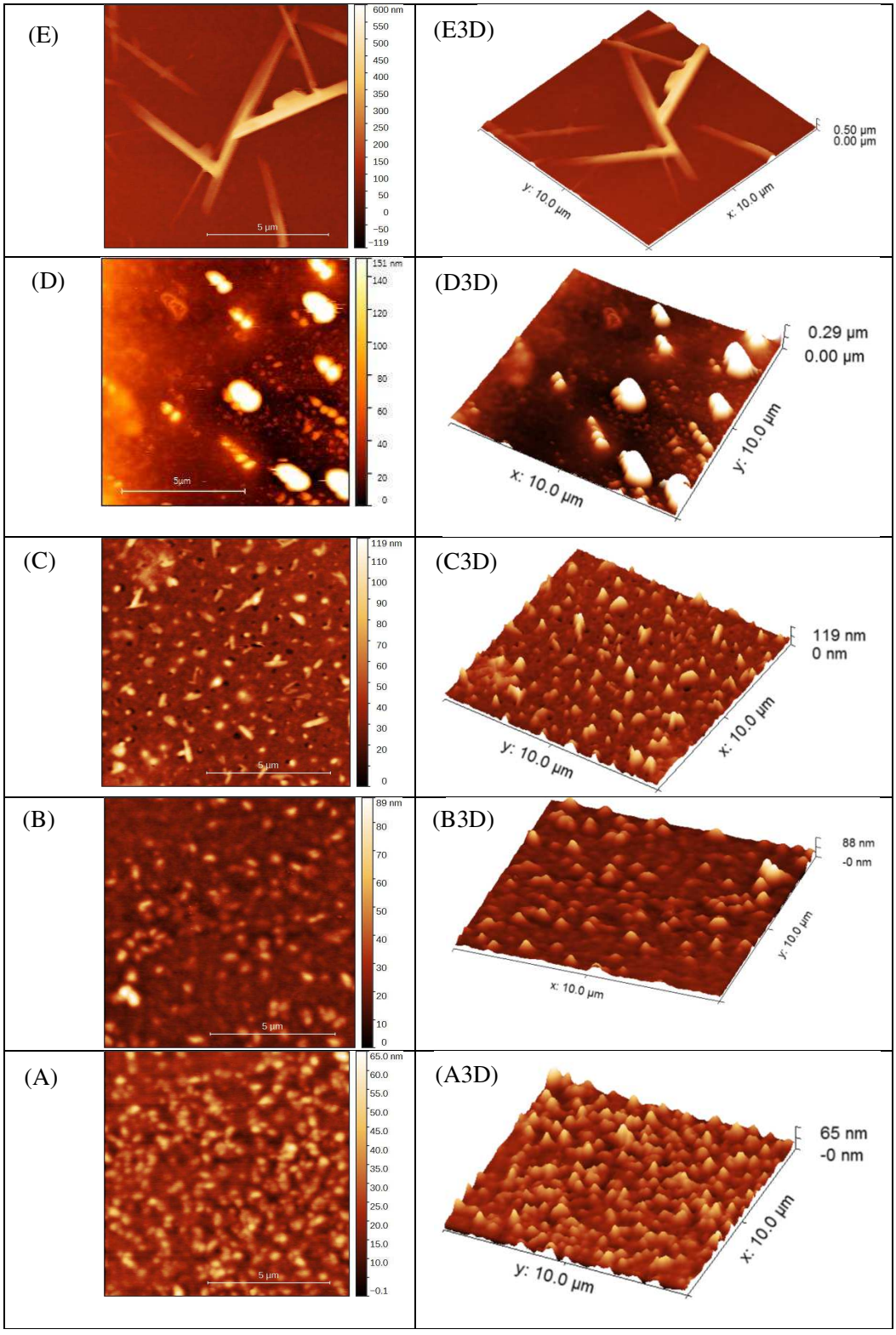
(E)
600 nm
550
500
450
400
350
300
250
200
150
100
50
0
−50
−119
5 µm
(E3D)
0.50 µm
0.00 µm
y: 10.0 µm
x: 10.0 µm
(D)
151 nm
140
120
100
80
60
40
20
0
5µm
(D3D)
0.29 µm
0.00 µm
x: 10.0 µm
y: 10.0 µm
(C)
119 nm
110
100
90
80
70
60
50
40
30
20
0
5 µm
(C3D)
119 nm
0 nm
y: 10.0 µm
x: 10.0 µm
(B)
89 nm
80
70
60
50
40
30
20
10
0
5 µm
(B3D)
88 nm
-0 nm
x: 10.0 µm
y: 10.0 µm
(A)
65.0 nm
60.0
55.0
50.0
45.0
40.0
35.0
30.0
25.0
20.0
15.0
10.0
−0.1
5 µm
(A3D)
65 nm
-0 nm
y: 10.0 µm
x: 10.0 µm

Fig. 5

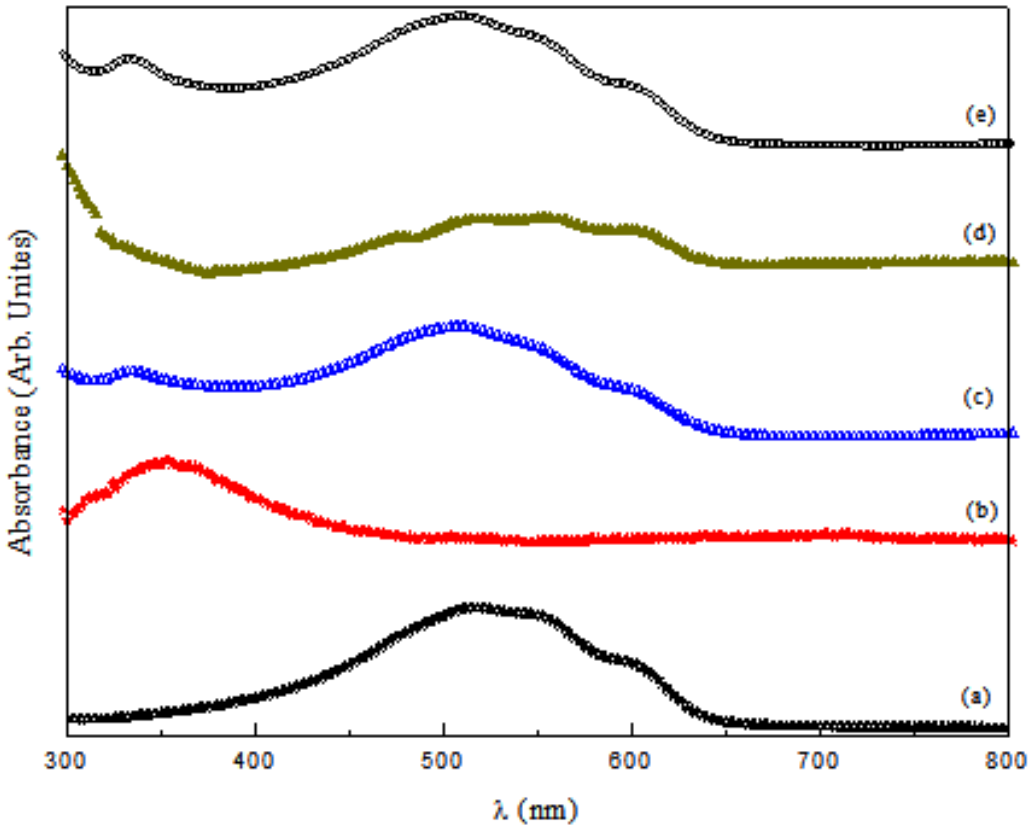

Fig. 6

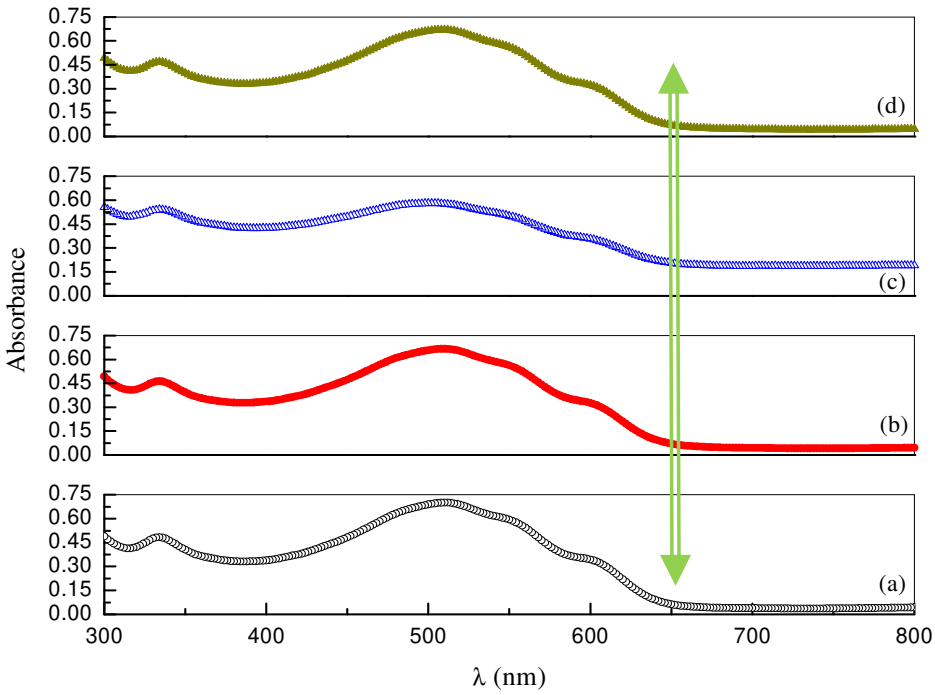
Absorbance
0.75
0.60
0.45
0.30
0.15
0.00
(d)
(c)
(b)
(a)
300
400
500
600
700
800
λ (nm)

Fig. 7

(c)

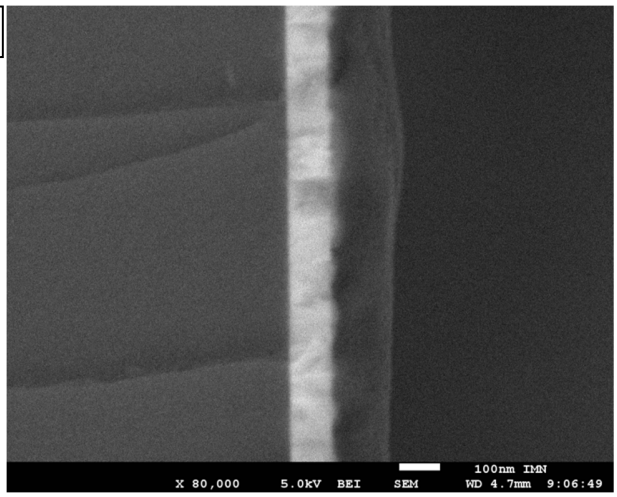
X 80,000 5.0kV BEI SEM
100nm IMN
WD 4.7mm 9:06:49

(b)

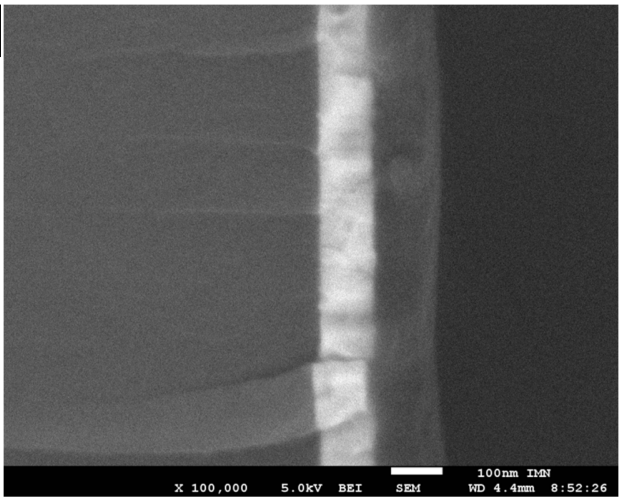
X 100,000 5.0kV BEI SEM
100nm IMN
WD 4.4mm 8:52:26

(a)

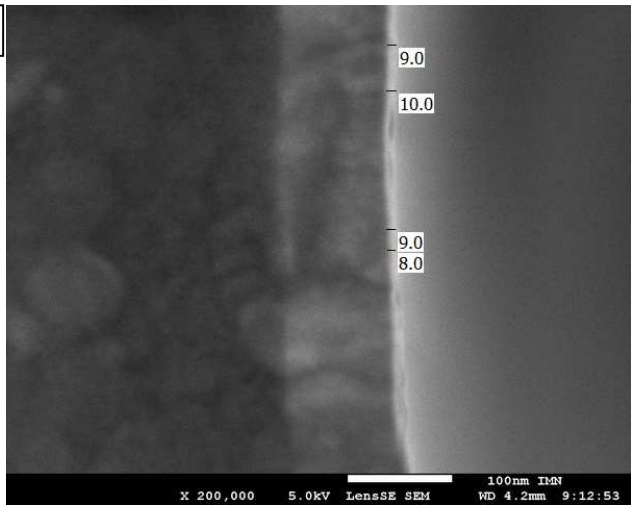
9.0
10.0
9.0
8.0
X 200,000 5.0kV LensSE SEM
100nm IMN
WD 4.2mm 9:12:53

Fig. 8

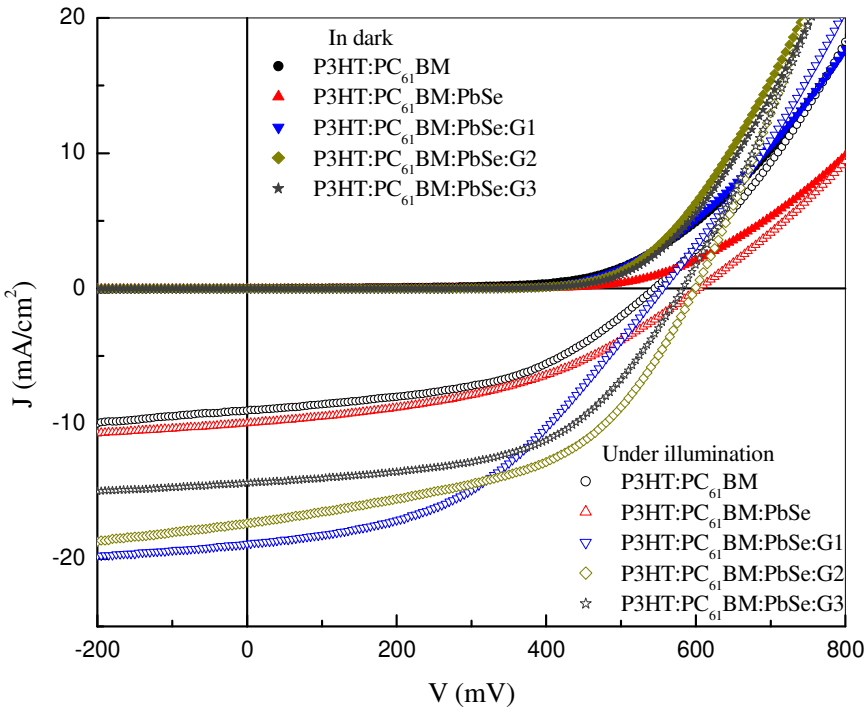
In dark
P3HT:PC61BM
P3HT:PC61BM:PbSe
P3HT:PC61BM:PbSe:G1
P3HT:PC61BM:PbSe:G2
P3HT:PC61BM:PbSe:G3
Under illumination
P3HT:PC61BM
P3HT:PC61BM:PbSe
P3HT:PC61BM:PbSe:G1
P3HT:PC61BM:PbSe:G2
P3HT:PC61BM:PbSe:G3
J (mA/cm2)
V (mV)
20
10
0
-10
-20
-200
0
200
400
600
800

Fig. 9

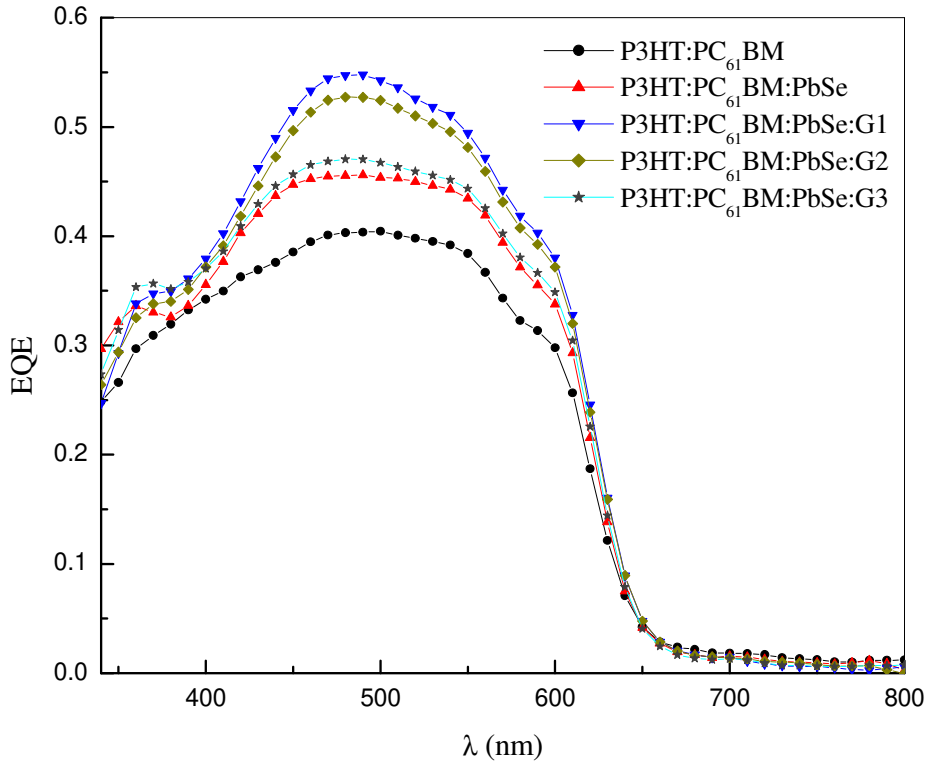
0.6
0.5
0.4
0.3
0.2
0.1
0.0
EQE
400
500
600
700
800
λ (nm)
P3HT:PC61BM
P3HT:PC61BM:PbSe
P3HT:PC61BM:PbSe:G1
P3HT:PC61BM:PbSe:G2
P3HT:PC61BM:PbSe:G3

Fig. 10

Table caption

Table 1 Photovoltaic parameters for fabricated BHJ solar cells with different active layers

Table 1

Active layer	V_{oc}(V)	J_{sc}(mA/cm^2)	FF (%)	*PCE*(%)	R_s (Ω)	R_{sh} (Ω)	RMS (nm)
P3HT:PC_{61}BM	0.55	9.03	47.23	2.32	10	224	7
P3HT:PC_{61}BM:PbSe	0.60	9.97	42.71	2.57	16	249	8
P3HT:PC_{61}BM:PbSe:G1	0.56	18.89	43.40	4.55	10	199	12
P3HT:PC_{61}BM:PbSe:G2	0.60	17.35	49.65	5.16	6	142	38
P3HT:PC_{61}BM:PbSe:G3	0.58	14.37	53.58	4.49	7	313	67

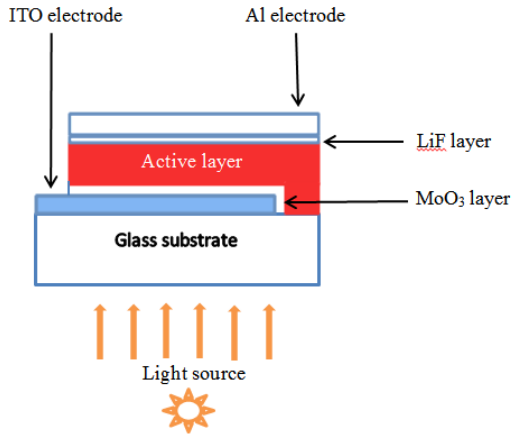
ITO electrode
Al electrode
Active layer
LiF layer
MoO3 layer
Glass substrate
Light source

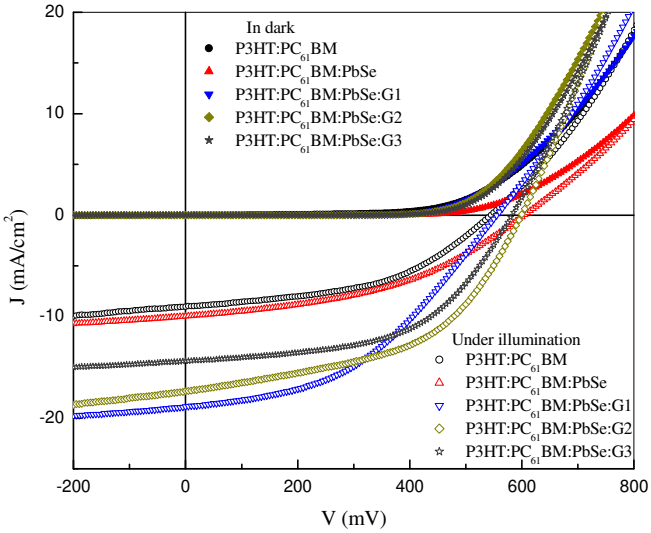
In dark
P3HT:PC61BM
P3HT:PC61BM:PbSe
P3HT:PC61BM:PbSe:G1
P3HT:PC61BM:PbSe:G2
P3HT:PC61BM:PbSe:G3
Under illumination
P3HT:PC61BM
P3HT:PC61BM:PbSe
P3HT:PC61BM:PbSe:G1
P3HT:PC61BM:PbSe:G2
P3HT:PC61BM:PbSe:G3
J (mA/cm2)
V (mV)
20
10
0
-10
-20
-200
0
200
400
600
800